

**Beyond modelocking: High repetition-rate frequency
combs derived from a continuous-wave laser**

by

Daniel C. Cole

B.S., Washington University in St. Louis, 2012

M.S., University of Colorado, 2015

A thesis submitted to the
Faculty of the Graduate School of the
University of Colorado in partial fulfillment
of the requirements for the degree of
Doctor of Philosophy
Department of Physics
2018

This thesis entitled:
Beyond modelocking: High repetition-rate frequency combs derived from a continuous-wave laser
written by Daniel C. Cole
has been approved for the Department of Physics

Scott A. Diddams

Reader Two

Date _____

The final copy of this thesis has been examined by the signatories, and we find that both the content and the form meet acceptable presentation standards of scholarly work in the above mentioned discipline.

Cole, Daniel C. (Ph.D., Physics)

Beyond modelocking: High repetition-rate frequency combs derived from a continuous-wave laser

Thesis directed by Dr. Scott A. Diddams

Optical frequency combs based on modelocked lasers have revolutionized precision metrology by facilitating measurements of optical frequencies, with implications both for fundamental scientific questions and for applications such as fast, broadband spectroscopy. In this thesis, I describe advances in the generation of frequency combs without modelocking in platforms with smaller footprints and higher repetition rates, with the ultimate goal of bringing frequency combs to new applications in a chip-integrated package. I discuss two approaches for comb generation: parametric frequency conversion in Kerr microresonators and active electro-optic modulation of a continuous-wave laser. After introducing microresonator-based frequency combs (microcombs), I discuss two specific developments in microcomb technology: First, I describe a new, extremely reliable method for generation of soliton pulses through the use of a phase-modulated pump laser. This technique eliminates the dependence on initial conditions that was formerly a universal feature of these experiments, presenting a solution to a significant technical barrier to the practical application of microcombs. Second, I present observations of *soliton crystal* states with highly structured ‘fingerprint’ optical spectra that correspond to ordered pulse trains exhibiting crystallographic defects. These pulse trains arise through interaction of solitons with avoided mode-crossings in the resonator spectrum. I also discuss generation of Kerr soliton combs in the Fabry-Perot (FP) geometry, with a focus on the differences between the FP geometry and the ring geometry that has been the choice of most experimenters to date. Next, I discuss combs based on electro-optic modulation. I introduce the operational principle, and then describe the first self-referencing of a frequency comb of this kind and a proof-of-principle application experiment. Finally, I discuss a technique for reducing the repetition rate of a high repetition-rate frequency comb, which will be a necessary post-processing step for some applications.

Contents

1	Generation and control of single microresonator solitons using a phase-modulated pump laser	1
1.1	Theoretical investigation of soliton generation with a phase-modulated pump laser	2
1.2	Spontaneous generation of single solitons using a phase-modulated pump laser	6
1.3	Soliton control using a phase-modulated pump laser	8
1.4	Subharmonic phase modulation for high repetition-rate systems	11
2	Microresonator-based frequency combs: Summary and outlook	14
References		17

Figures

1.1	Energy-level diagram with a phase-modulated pump laser	2
1.2	Quasi-CW background in a PM-pumped resonator	4
1.3	Mechanism for soliton generation with a PM pump	5
1.4	Experimental setup for soliton generation with a phase-modulated pump laser	7
1.5	Spontaneous generation of solitons using a phase-modulated pump laser	8
1.6	Repetition-rate control using a phase-modulated pump laser	9
1.7	Repetition-rate switching driven by a phase-modulated pump laser	10
1.8	Subharmonic phase modulation for high repetition-rate soliton generation	12

Chapter 1

Generation and control of single microresonator solitons using a phase-modulated pump laser

This chapter discusses the direct generation and control of single solitons in optical microring resonators using a pump laser phase modulated at a frequency near the resonator's free spectral range. Based on a proposal by Taheri, Eftekhar, and Adibi in 2015 [1], these results present a promising new method for simple and deterministic generation of single solitons. We build on a body of work describing past applications of pump-laser modulation to facilitate the generation of microresonator solitons. Lobanov et al. demonstrated that phase and/or intensity modulation can enable deterministic condensation of either one or zero solitons from an extended modulation-instability pattern [2], and transient bursts of phase modulation [3] and amplitude modulation [4] have been used to directly excite solitons in fiber-ring resonators. Control of fiber-ring solitons by phase modulation has been demonstrated in similar experiments [5]. Generation of solitons using a train of pump pulses with repetition-rate matched to the resonator FSR has also been demonstrated [6]. The work we present here builds on these previous demonstrations by reducing the complexity of the scheme; all that is required is sinusoidal phase modulation of the pump with reasonably low modulation index, and no transient perturbation to the system parameters is necessary.

We begin by presenting theoretical investigations into the effect of phase modulation (PM) at the resonator free-spectral range on solitons in microresonators, and then we demonstrate deterministic generation and control of single solitons using pump-laser phase modulation.

1.1 Theoretical investigation of soliton generation with a phase-modulated pump laser

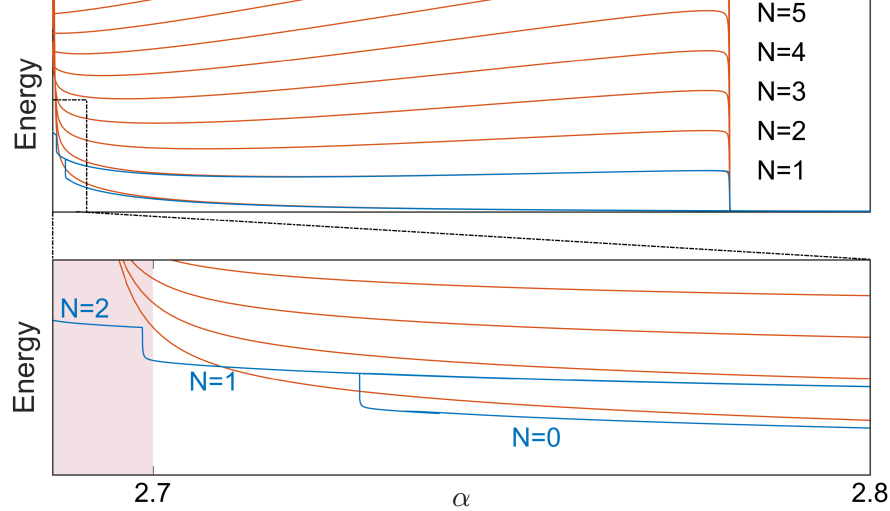


Figure 1.1: **Energy-level diagram with a phase-modulated pump laser.** An energy-level diagram with a phase-modulated pump laser (blue levels), on top of the diagram for a CW laser from Fig. ???. Phase modulation eliminates the degeneracy between the $N = 1$ level and all other levels over a range of detunings near the minimum detuning for solitons, and also precludes the existence of stable multi-soliton ensembles over the majority of the range where solitons are supported. Although the interval over which N is restricted to 1 is fairly narrow, we find that it is readily accessible in experiment. Simulations indicate that non-stationary solutions are degenerate with the $N = 2$ level for $\alpha \leq 2.7$; this region is highlighted with the red shading. The level-diagram is created using an LLE simulation with $F^2 = 4$, $\beta_2 = -0.0187$ (chosen to match the dispersion of the resonator used for experiments), and $\delta_{PM} = \pi$.

To theoretically explore the physics of soliton generation with PM pumping¹, we use the LLE with a modified driving term that incorporates the effect of phase modulation [1]:

$$\frac{\partial \psi}{\partial \tau} = -(1 + i\alpha)\psi + i|\psi|^2\psi - i\frac{\beta_2}{2}\frac{\partial^2 \psi}{\partial \theta^2} + Fe^{i\delta_{PM} \cos \theta}. \quad (1.1)$$

Here δ_{PM} represents the phase-modulation index, which describes the phase-modulated input field according to $E_{PM} = E_0 e^{i\delta_{PM} \cos(2\pi f_{PM} t)}$; $f_{PM} \sim f_{FSR}$ is the frequency of the applied phase modulation.

Simulations of Eq. 1.1 reveal that PM transforms the resonator excitation spectrum from a series of $N = 0, 1, 2, \dots$ up to N_{max} solitons to a single level $N = 1$ near threshold, eliminating

¹ I gratefully acknowledge the contributions of Miro Erkintalo, who originated the approximation of the derivatives of ϕ as zero and suggested the mechanism of locally-vanishing bistability for soliton generation.

degeneracy between these states as shown in Fig. 1.1. This occurs due to spatial variations of effective loss and detuning parameters that result from the phase modulation. We can obtain an approximation for these parameters by inserting the ansatz $\psi(\theta, \tau) = \phi(\theta, \tau)e^{i\delta_{PM} \cos \theta}$ and the requirement that $\partial\psi/\partial\tau = 0$ into Eq. 1.1 [5]. By expanding the second-derivative term and setting derivatives of ϕ to zero we arrive at an equation for the quasi-CW background in the PM-pumped resonator:

$$F = (\gamma(\theta) + i\eta(\theta))\phi - i|\phi|^2\phi, \quad (1.2)$$

where the spatially-varying effective loss and detuning terms have been defined as:

$$\gamma(\theta) = 1 + \frac{\beta_2}{2}\delta_{PM} \cos \theta, \quad (1.3)$$

$$\eta(\theta) = \alpha - \frac{\beta_2}{2}\delta_{PM}^2 \sin^2 \theta. \quad (1.4)$$

This equation immediately yields an approximation for the stationary solution ψ_s :

$$\psi_s(\theta) = \frac{Fe^{i\delta_{PM} \cos \theta}}{\gamma(\theta) + i(\eta(\theta) - \rho(\theta))}, \quad (1.5)$$

where $\rho(\theta) = |\phi(\theta)|^2$ is the (smallest real) solution to the cubic polynomial that results from taking the modulus-square of Eq. 1.2:

$$F^2 = \left[\gamma(\theta)^2 + (\eta(\theta) - \rho(\theta))^2 \right] \rho(\theta). \quad (1.6)$$

In neglecting spatial derivatives of ϕ but retaining the derivatives of the phase term $e^{i\delta_{PM} \cos \theta}$ we have made the approximation that the dominant effect of dispersion comes from its action on the existing broadband phase-modulation spectrum. This model reveals that amplitude variations in the quasi-CW background can be expected as a result of the spatially-varying effective loss and detuning terms that arise from phase modulation of the pump laser.

Fig. 1.2 shows the predictions of simulations of Eq. 1.1 (color) and the analytical model Eq. 1.6 (black). The two agree quantitatively for weak modulation ($\delta_{PM} = \pi/2$, blue) and qualitatively with larger depth ($\delta_{PM} = 4\pi$, green); both indicate that the field ψ exhibits amplitude variations due to the spatially-varying effective loss and detuning. This phenomenon suggests an explanation

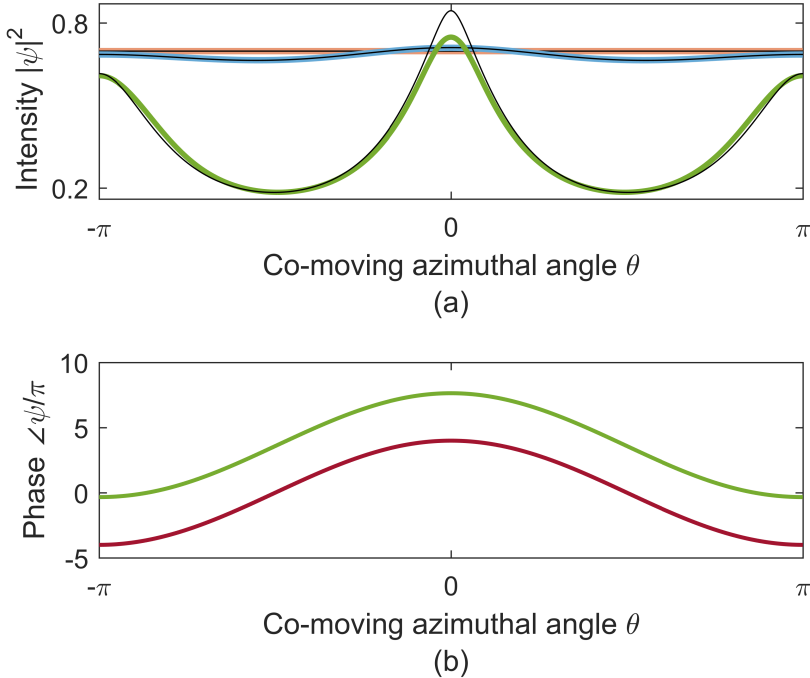


Figure 1.2: **Quasi-CW background in a PM-pumped resonator.** (a) Simulated intensity of the background in the resonator without (orange) and with PM of depth $\delta_{PM} = \pi/2$ (blue) and $\delta_{PM} = 4\pi$ (green), with analytical approximations in black. Here α is slightly larger than the critical value for soliton formation. (b) Phase profile of the field ψ corresponding to the green trace in (a) with $\delta_{PM} = 4\pi$, and the phase profile of the driving term $F e^{i\delta_{PM} \cos \theta}$ (red) with modulation depth 4π . The phase of the field is very nearly the phase of the drive plus a constant offset.

for the spontaneous formation of a single soliton as the detuning α is decreased in terms of the local disappearance of Kerr bistability.

As discussed in Sec. ??, for the LLE with a CW pump the background field ψ_{CW} can take one of two stable values over a range of the parameters α and F^2 . This leads to the emergence of a tilted resonance lineshape like the one shown in Fig. 1.3a, with an effectively red-detuned branch lying at higher values of α , an effectively blue-detuned branch lying at lower values of α , and an interval in α over which they both exist and the system is bistable (recall that the middle branch is unstable). With spatially-varying effective loss and detuning terms, the field $\psi_s(\theta)$ described by Eq. 1.5 now takes a value at each point in the cavity that is determined by the local parameters $\gamma(\theta)$ and $\eta(\theta)$, with the result that each point lies on its own effective resonance. The resulting resonance *surface* is

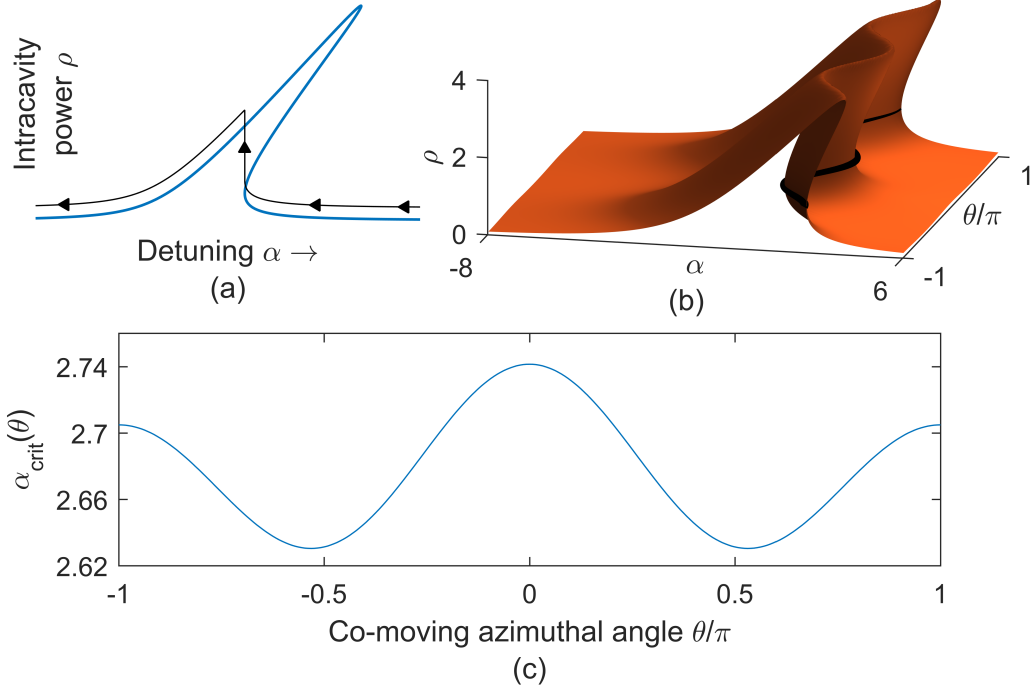


Figure 1.3: Mechanism for soliton generation with a PM pump. (a) Plot of a Kerr-shifted resonance, here with $F^2=12$. The CW background field ψ_{CW} follows the black curve in an increasing-frequency scan of the pump laser (although actually a portion of the upper branch is unstable due to modulation instability above threshold). (b) For the case of a phase-modulated pump, the field $\psi_s(\theta)$ at each point θ lies on a qualitatively similar resonance that is defined locally by $\gamma(\theta)$ and $\eta(\theta)$, with the result that a resonance surface emerges. The resonance surface is shown here for $F^2 = 4$, $\beta_2 = -0.0187$, and $d_{PM} = 4\pi$, which is chosen to accentuate the θ -dependence. The curve $\alpha_{crit}(\theta)$ is shown in black. (c) A plot of the value $\alpha_{crit}(\theta)$ at which the Kerr bistability locally vanishes and the field $\psi_s(\theta)$ must jump to the effectively blue-detuned branch, associated with the vertical transition in (a), for $F^2 = 4$, $\beta_2 = -0.0187$, and $\delta_{PM} = \pi$. The value $\alpha_{crit}(\theta = 0)$ can be used to approximate the detuning at which a soliton is generated in an increasing-frequency scan of the pump laser; the input parameters here match the level diagram in Fig. 1.1.

shown in Fig. 1.3b. It can be independently determined for each point in the cavity whether $\psi_s(\theta)$ exhibits bistability. Applying the analysis presented in Sec. ?? to Eq. 1.6, we identify the value of ρ associated with the disappearance of the bistability in a decreasing- α scan as the smaller value ρ_- at which $\partial F^2 / \partial \rho = 0$:

$$\rho_- = \left(2\eta - \sqrt{\eta^2 - 3\gamma^2} \right) / 3, \quad (1.7)$$

For fixed F^2 the function $\alpha_{crit}(\theta)$ describing the critical value of α at which the bistability ends is

found by numerically solving the implicit equation for α_{crit} obtained by inserting ρ_- into Eq. 1.2:

$$F^2 = \left[\gamma^2(\theta) + (\eta(\theta) - \rho_-(\theta))^2 \right] \rho_-(\theta), \quad (1.8)$$

where $\alpha_{crit}(\theta)$ is included via $\eta(\theta) = \alpha_{crit}(\theta) - \frac{\beta_2}{2} \delta_{PM}^2 \sin^2 \theta$. Fig. 1.3c shows a calculation of $\alpha_{crit}(\theta)$ for $F^2 = 4$ and $\beta_2 = -0.0187$, which is chosen to match the dispersion of the resonator used for the experiments presented below. For $\theta = 0$ this calculation predicts disappearance of the bistability, and subsequent soliton generation, at $\alpha = 2.741$, which is a difference of 0.4 % from the value $\alpha = 2.729$ observed in the simulation presented in Fig. 1.1. The same calculation predicts disappearance of the bistability for $\theta = \pi$, at which point a second soliton is generated, at $\alpha = 2.705$, which is also in close agreement with the simulation.

1.2 Spontaneous generation of single solitons using a phase-modulated pump laser

We demonstrate deterministic generation of single solitons without condensation from an extended pattern in a 22-GHz FSR silica microdisk resonator. This resonator has $\Delta\nu \sim 1.5$ MHz linewidth, and was fabricated using a chemical etching process at CalTech [7]. We generate a frequency-agile laser for pumping the resonator by passing a CW seed laser through a single-sideband modulator (SSB) that is driven by a voltage-controlled oscillator (VCO) [8]. The seed laser is extinguished in the modulator and the resulting sideband can be swept by adjusting the voltage applied to the VCO; sweeping rates up to 100 GHz/ μ s over a range over 4 GHz are possible. The pump laser is phase-modulated with index $\delta_{PM} \sim \pi$ and amplified to normalized power F^2 between 2 and 6. The pump-laser detuning $\nu_0 - \nu_p$, where ν_0 is the frequency of the pumped mode and ν_p is the frequency of the pump laser, is measured in real time using an AOM-shifted probe beam as shown in Fig. 1.4, and the high-bandwidth feedback allowed by the VCO/SSB scheme allows thermal instabilities associated with the red detuning that is required for soliton generation to be overcome.

To generate single solitons, we begin with large red detuning $\nu_0 - \nu_p = 40$ MHz and decrease the detuning until a soliton is generated near $\nu_0 - \nu_p \sim 5$ MHz detuning; this value depends on the

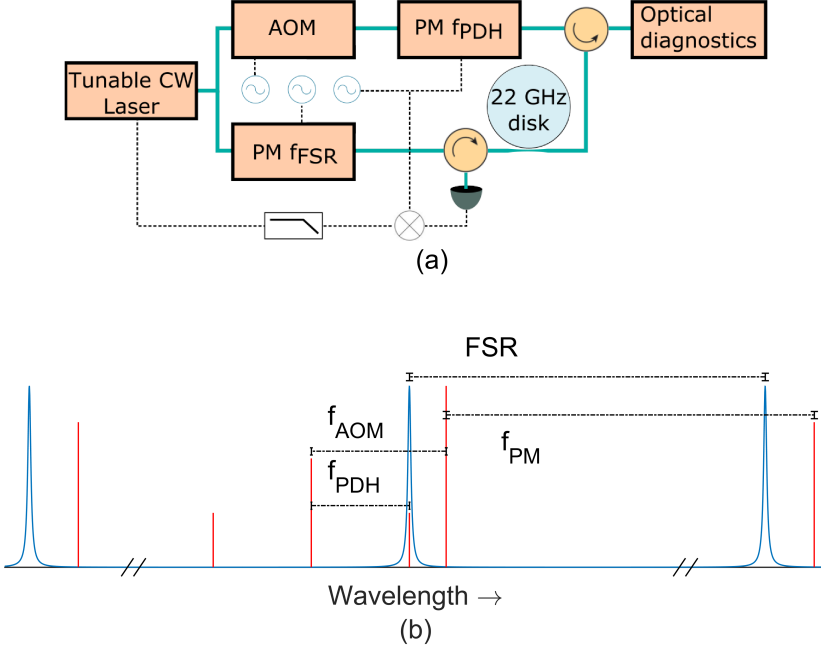


Figure 1.4: Experimental setup for soliton generation with a phase-modulated pump laser. (a) Schematic diagram of the experimental setup, including the pump laser phase-modulated at frequency $f_{PM} \sim f_{FSR}$ and an AOM-shifted probe beam that is modulated at frequency f_{PDH} for implementation of a Pound-Drever-Hall sideband lock. The probe beam addresses the resonator in the counter-propagating direction. (b) Frequency-domain diagram of the scheme used to maintain stable red detuning of the pump laser. As f_{PDH} is increased, the detuning α is decreased.

pump power and coupling condition. We measure the power converted by the Kerr nonlinearity to new frequencies by passing a portion of the resonator's output through an optical band-reject filter that attenuates the power at frequencies corresponding to the phase-modulated pump laser. This 'comb power' measurement reveals a step upon soliton formation, as shown in Fig. 1.5a, after which we can measure the soliton spectrum with phase-modulation sidebands on the pump shown in Fig. 1.5b. After soliton generation, we observe that the soliton can be preserved while the detuning is increased again, consistent with Fig. 1.1. Additionally, we observe that it is possible to turn off the phase modulation without loss of the soliton, in agreement with the simulations presented in Ref. 1.

Automating soliton generation by repeatedly scanning the laser into resonance ($\nu_0 - \nu_p \sim 5$ MHz) and back out again ($\nu_0 - \nu_p \sim 20$ MHz, far enough that the soliton is lost) has enabled reversible generation of 1000 solitons in 1000 trials over 100 seconds, with a measured 100 % success rate. Our

probe beam allows measurement of the detuning at which soliton generation occurs, which changes little from run to run. We present a histogram of detuning measurements for the generation of 160 solitons in Fig. 1.5c.

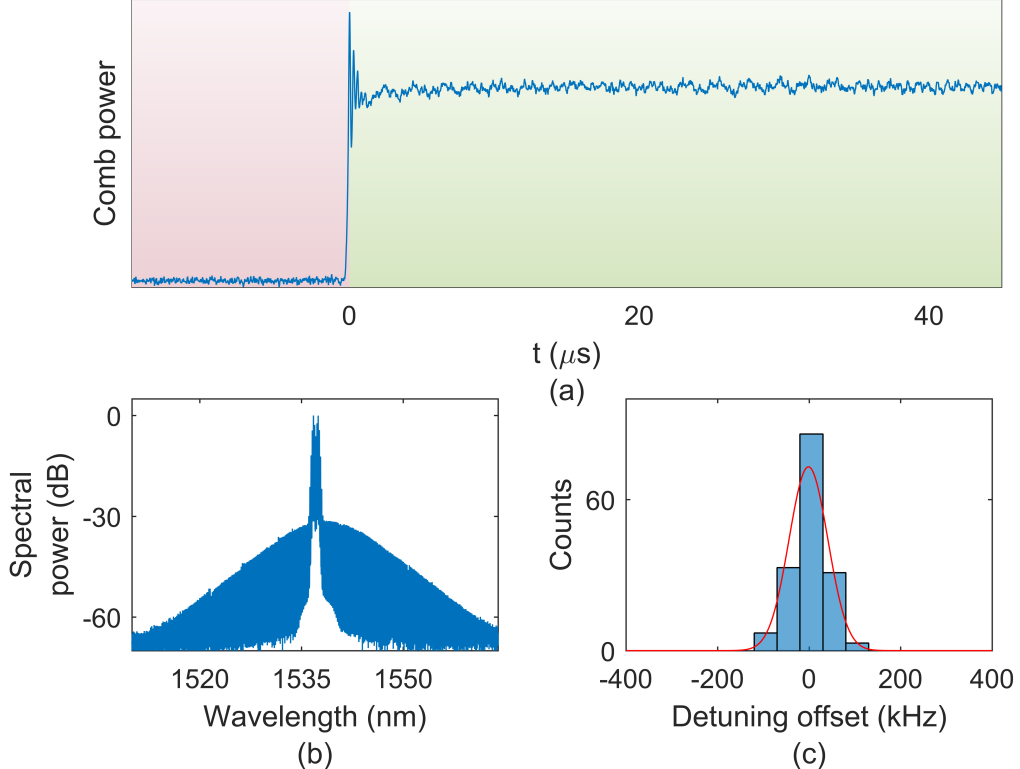


Figure 1.5: Spontaneous generation of solitons using a phase-modulated pump laser. (a) ‘Comb power’ trace obtained by filtering the pump laser out of the spectrum of light transmitted past the resonator, indicating a discrete step in the amount of frequency-converted light upon direct generation of a soliton. (b) Optical spectrum of a spontaneously generated soliton. The spectrum of the phase-modulated pump laser is visible as the set of higher-amplitude lines in the center. (c) Histogram of measured detuning values at which a soliton is generated relative to a reference (mean) value over 160 trials.

1.3 Soliton control using a phase-modulated pump laser

In addition to enabling deterministic generation of single solitons, phase modulation of the pump laser also facilitates timing and repetition-rate control of the resulting out-coupled pulse train. We characterize this control by measuring the repetition rate of the soliton pulse train as

the phase-modulation frequency is varied. This measurement is conducted as follows: First, we photodetect the pulse train after removing the central spectral lines corresponding to the phase-modulated pump laser using an optical band-reject filter. Then, in order to obtain a measurement trace of the repetition rate as a function of time, the photodetected signal is mixed with a local oscillator to reduce the signal frequency from f_{rep} to ~ 1 MHz, after which a spectrogram of the resulting waveform is calculated.

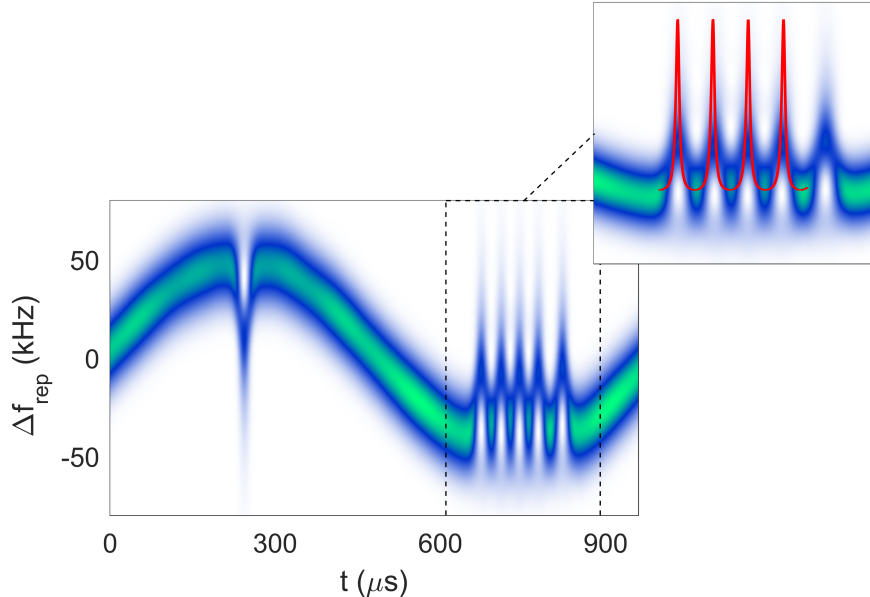


Figure 1.6: Repetition-rate control using a phase-modulated pump laser. Spectrogram of the measured repetition rate of the soliton pulse train generated by a phase-modulated pump laser as the frequency of phase modulation is swept through ± 50 kHz over 1 ms. Glitches in the spectrogram indicate that the range over which f_{rep} can be locked to f_{PM} has been exceeded. Inset: Qualitative agreement with simulations when f_{PM} is outside of the locking bandwidth, shown in red. As the soliton and the pump phase evolve at different frequencies f_{rep} and f_{PM} , the soliton periodically approaches the maximum of the phase profile. The soliton's group velocity changes, nearly locking to the phase modulation, before becoming clearly unlocked again.

Fig. 1.6 shows the measured repetition rate f_{rep} as f_{PM} is swept sinusoidally through a range of ± 50 kHz around the soliton's natural repetition rate; the repetition rate follows the PM except for glitches near the peaks of the sweep when $f_{PM} - f_{rep}$ exceeds a locking bandwidth of about ± 40 kHz. This observation is consistent with an estimate of the locking range $\delta_{PM} \times D_2/2\pi \sim 44$ kHz that is presented in Ref. [5], where we have used the approximate value $D_2 = 14$ kHz/mode

$(\beta_2 = -2D_2/\Delta\omega = -0.0187$, via $\Delta\nu \sim 1.5$ MHz). In the inset of Fig. 1.6 we overlay the results of LLE simulations that qualitatively match the observed behavior. These simulations are conducted by introducing the term $+\beta_1 \frac{\partial\psi}{\partial\theta}$ to the right-hand side of Eq. 1.1, where $\beta_1 = -2(f_{FSR} - f_{PM})/\Delta\nu$ incorporates a difference between the modulation frequency and the FSR of the resonator into the model; β_1 may be varied in time to simulate the sweep of f_{PM} . These simulations indicate that the periodic nature of the glitches is due to the residual pulling of the phase modulation on the soliton when the latter periodically cycles through the pump's phase maximum.

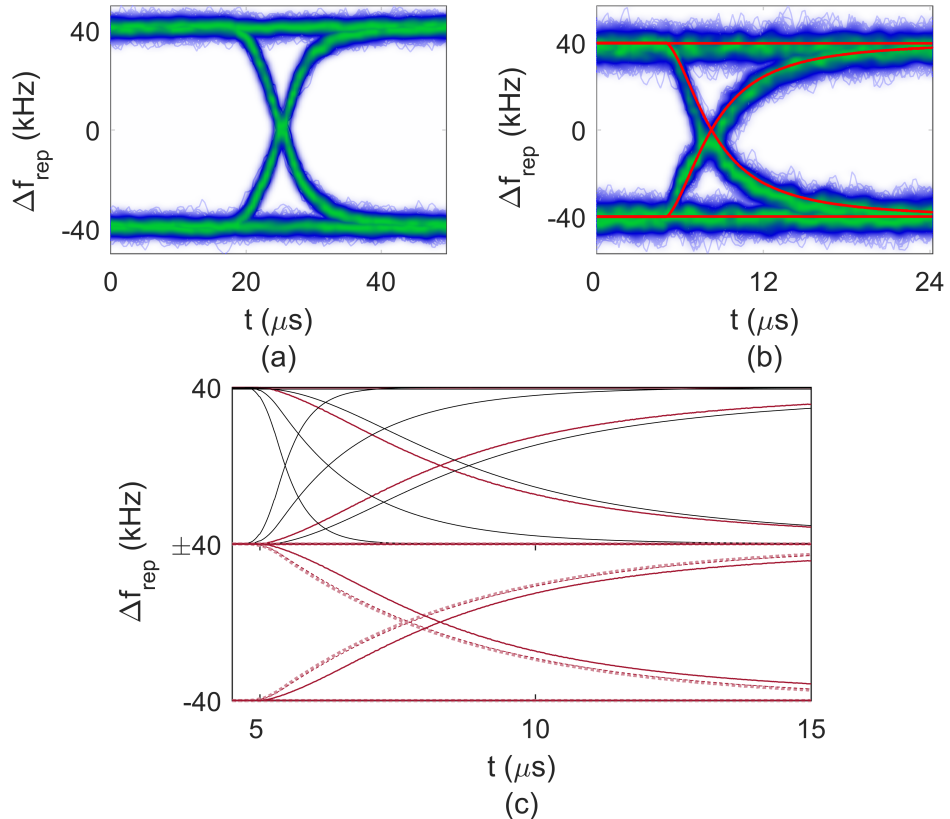


Figure 1.7: **Repetition-rate switching driven by a phase-modulated pump laser.** (a) Measured eye-diagram showing the switching capability of the soliton pulse train's repetition rate as f_{PM} is switched over ± 40 kHz with $10 \mu s$ transition time. (b) The same with 60 ns transition time, with an LLE simulation of the dynamics (red) overlaid. The simulation parameters are $\delta_{PM} = 0.9\pi$, $\Delta\nu = 1.5$ MHz. (c) Simulated switching dynamics for various linewidths and modulation depths. Top: $\Delta\nu = 10$ MHz (fastest, left), 3 MHz, and 1.4 MHz (traces shown in solid black). Bottom: depths of 2π and 6π (dashed red, curves nearly overlap). In each, the other parameter matches the simulation in (c), which is shown again in solid red.

To evaluate the utility of phase modulation for fast control of the soliton's properties, we

measure the repetition rate of the pulse train as f_{PM} is rapidly switched by ± 40 kHz, which is within the soliton's locking range. To measure these fast dynamics, we split the photodetected repetition-rate signal and send one path through a reactive circuit element (a set of low-pass filters) that induces a frequency-dependent phase shift. By comparing the phase between the two paths as a function of time, the time-dependent repetition rate can be determined. We construct eye-diagrams out of the resulting data; these are shown in Fig. 1.7. In Fig. 1.7a, f_{PM} is switched with $200\ \mu s$ period and $10\ \mu s$ transition time; in Fig. 1.7b it is switched with $100\ \mu s$ period and $60\ ns$ transition time. These eye diagrams show that the PM enables exquisite control of the soliton pulse train.

We overlay a simulated eye diagram on the data in Fig. 1.7b. This simulation is conducted for parameters $\Delta\nu = 1.5$ MHz, $\delta_{PM} = 0.9\pi$ that are near the experimental values, and the agreement between measurement and simulation indicates that the measurements are consistent with fundamental LLE dynamics. Fig. 1.7c presents the results of additional LLE simulations; the basic result is that the switching speed of f_{rep} is limited by the resonator linewidth, and can be only modestly improved by increasing δ_{PM} .

1.4 Subharmonic phase modulation for high repetition-rate systems

One apparent barrier to the use of a phase-modulated pump laser for single-soliton generation and manipulation is the electronically-inaccessible FSRs of some typical microcomb resonators. However, it is possible to overcome this challenge by phase modulating at a subharmonic of the FSR. Simulations indicate that PM can directly excite single solitons with small modulation depth, e.g. $\delta_{PM} = 0.15\pi$. In this limit, only the first-order PM sidebands are relevant, and their amplitude and phase relative to the carrier control the dynamics. For a small desired modulation depth defined by the relationship between the first-order sidebands and the carrier, it is possible to modulate at a frequency $f_{PM} \sim f_{FSR}/N$ so that the N^{th} -order PM sidebands and the carrier address resonator modes with relative mode numbers -1, 0, and 1. The depth of modulation at the frequency f_{PM} can be chosen to fix the amplitudes of the N^{th} -order PM sidebands relative to the carrier and target a desired effective modulation depth. It is worth noting that when N is odd, phase modulation

is recovered when the sidebands of order $-N$, 0, and N address resonator modes -1, 0, and 1. When N is even the result is pure amplitude modulation, such that the driving term takes the form $F(1 + A \cos \theta)$. Simulations indicate that this AM profile also enables spontaneous single-soliton generation under some circumstances, but we note that this modulation profile cannot be obtained from a standard Mach-Zehnder modulator, which provides a drive like $F \cos(\eta + \delta \cos \theta)$; AM in general may be less useful than PM because schemes of comparable complexity do not always provide robust trapping of solitons to the same point in the co-moving frame at which they are generated [9].

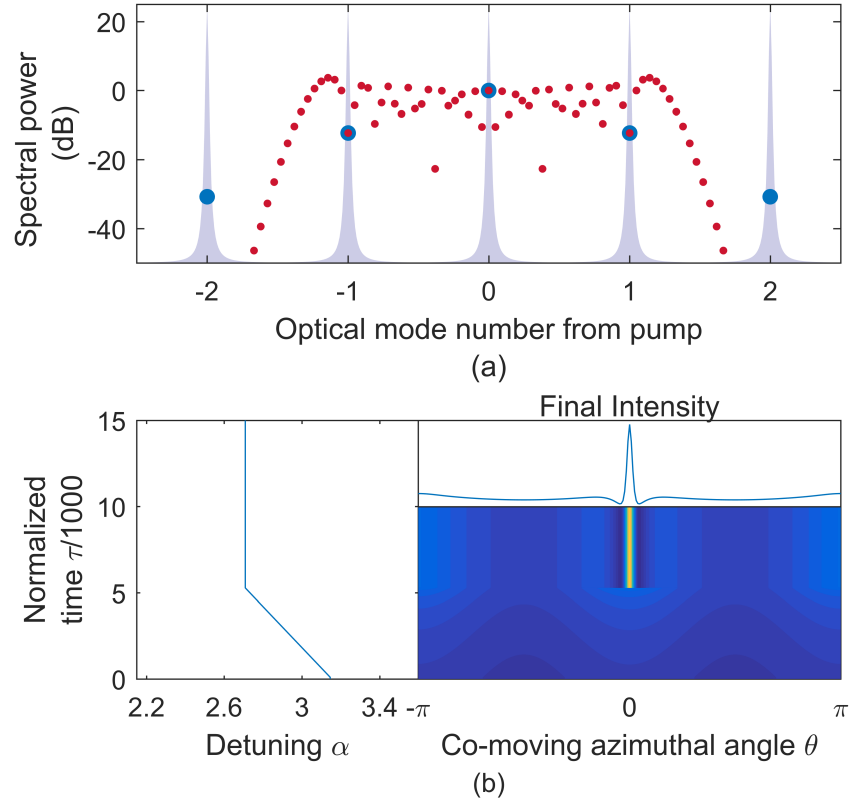


Figure 1.8: Subharmonic phase modulation for high-repetition-rate soliton generation. (a) Spectra of PM at f_{FSR} with depth 0.15π (blue) and at $f_{FSR}/21$ with depth $\sim 8.3\pi$ (red). The relationships between the fields that address resonator mode numbers -1, 0, and 1 (as indicated by the gray Lorentzian curves) are the same in both cases. (b) LLE simulation of single-soliton generation using the subharmonic phase-modulation spectrum shown in red in panel (a). Only modes $n = 0, \pm 21, \pm 42, \dots$ of the phase-modulated driving field are coupled into the resonator and affect the LLE dynamics, with modes $|n| > 21$ having negligible power. As α is increased from a large initial value, a soliton is spontaneously generated, exactly as in the case of phase modulation near the FSR.

Fig. 1.8 presents an example of this technique. We simulate spontaneous soliton generation with PM at $f_{PM} = f_{rep}/N = f_{rep}/21$. The effective modulation depth is 0.15π , which requires real modulation depth at the frequency f_{PM} with depth $\delta_{PM} \sim 8.3\pi$. Because the phase modulation spreads the optical power into the PM sidebands, use of this technique requires higher optical power for the same effective pumping strength; in this example the optical power must be increased by ~ 15.6 dB. A smaller real modulation depth could have been chosen to recover effective depth of $\delta_{eff} = 0.15\pi$, but our chosen depth of $\sim 8.3\pi$ gives better efficiency due to the higher ratio of the power in modes $0, \pm 21$ to the total power in the spectrum. While the required modulation depth and pump power are higher with subharmonic phase modulation, neither is impractical. This technique could be used for spontaneous single-soliton generation in high-repetition rate systems; the example above indicates that it could be immediately applied in a 630 GHz-FSR resonator with 30 GHz phase modulation.

Chapter 2

Microresonator-based frequency combs: Summary and outlook

Chapters ??-?? discussed generation of frequency combs from a continuous-wave laser by parametric frequency conversion in Kerr-nonlinear resonators. I described three results: 1. The investigation and implementation of a technique for spontaneous soliton generation in Kerr resonators using a phase-modulated pump laser, 2. The observation and explanation of soliton crystals in Kerr resonators, and 3. A theoretical investigation of Kerr-comb generation in Fabry-Perot cavities, with an emphasis on the properties of solitons and soliton generation. These results help to more clearly define what is possible with these systems, and they suggest avenues for further research.

Soliton generation with a phase-modulated pump laser is a promising candidate for inclusion in chip-integrated Kerr-comb systems as the mechanism by which single-soliton operation is initiated. Two directions for continued work are additional analytical investigations into the full LLE with a phase-modulated pump, which could provide insight into the dynamics beyond what is possible using the approximations described in Chapter 1, and implementation of the technique with resonators that have electronically-inaccessible free-spectral ranges using the subharmonic-modulation approach that was proposed. Incorporation of the technique into a chip-integrated Kerr-soliton comb may also require modification and further development of the technique that was used to overcome thermal instabilities associated with the increasing-frequency pump-laser scan.

The investigation of soliton crystals presented is significant for several reasons. First, it represented an important step towards full explanation of observed Kerr-comb phenomena in terms of the LLE model. Second, soliton crystals have the attractive properties of single-soliton Kerr combs, with

the additional property that a soliton crystal of N pulses has conversion efficiency of pump-laser power into the comb that is roughly N times higher than a comparable single-soliton comb. With careful preparation of a particular crystal state, this could make them attractive for applications like optical arbitrary waveform generation and nonlinear spectroscopy. Additionally, soliton crystals present a hugely degenerate discrete configuration space that could be useful, for example, in implementations of an on-chip optical buffer [10] or in communications applications. Finally, experimental generation of soliton crystals is significantly simpler than generation of single solitons, where the change in the duty cycle of the optical waveform from extended pattern to single soliton leads to thermal instabilities that must be addressed through precise control of the pump-laser power and frequency. It is possible to propose a scheme for deterministic on-chip soliton crystal generation that makes use of two resonators, each constructed of looped single-mode optical waveguides. One resonator is pumped by a laser and hosts the soliton crystal. The second resonator need not be pumped, and exists to provide a specific perturbation to the mode structure of the first resonator to enable soliton crystallization; this could be achieved through careful engineering of the coupling between the resonators. If the free-spectral range of the second resonator is considerably higher than the free-spectral range of the first, and not near one of its harmonics, then realization of the single-mode perturbation to the mode structure of the first resonator that was assumed in Chapter ?? could be achieved. Implementing deterministic soliton crystal generation on a chip in this way could greatly simplify the requirements on the other components in a system for full-integration of Kerr solitons, as soliton generation could be achieved through slow tuning of the pump laser.

The theoretical investigation of Kerr-comb generation in the Fabry-Perot geometry will provide useful guidance for future experimental work. An obvious direction for continued work is the generation of solitons in Fabry-Perot cavities that make use of the additional degree of freedom provided by the dispersion applied by reflection at the ends of the cavity. This would build on previous experiments [6, 11]. In fact, soliton generation in Fabry-Perot cavities constructed of potted fiber ferrules with high-reflectivity end-coatings has already been realized at NIST Boulder [12], but there remains work to be done to achieve control of the total cavity dispersion with chirped

mirror-coatings. Unresolved questions include the effect of uncontrolled expansion of the mode in the coating on both the mirror reflectivity and its group-velocity dispersion. Looking to the chip scale, integrated Fabry-Perot cavities constructed of single-mode waveguides with photonic-crystal mirrors is a promising route for development that would further reduce the footprint of Kerr-comb systems. This work is ongoing at NIST Boulder, and primary comb has been observed in such a cavity [13]. Finally, I note that the proposal for deterministic chip-scale generation of soliton crystals presented above could be realized with two co-linear on-chip Fabry-Perot cavities, where the first cavity hosts the crystal, which is out-coupled in reflection, and the second cavity provides a perturbation to the first cavity's mode structure.

References

- [1] Hossein Taheri, Ali A. Eftekhar, Kurt Wiesenfeld, and Ali Adibi. Soliton formation in whispering-gallery-mode resonators via input phase modulation. *IEEE Photonics Journal* **7** (2015), 2200309 (cited on pages 1, 2, 7).
- [2] V. E. Lobanov, G. V. Lihachev, N. G. Pavlov, A. V. Cherenkov, T. J. Kippenberg, and M. L. Gorodetsky. Harmonization of chaos into a soliton in Kerr frequency combs. *Optics Express* **24** (2016), 27382 (cited on page 1).
- [3] Jae K Jang, Miro Erkintalo, Stuart G Murdoch, and Stéphane Coen. Writing and erasing of temporal cavity solitons by direct phase modulation of the cavity driving field. *Optics Letters* **40** (2015), 4755–4758 (cited on page 1).
- [4] Yadong Wang, Bruno Garbin, Francois Leo, Stephane Coen, Miro Erkintalo, and Stuart G. Murdoch. Writing and Erasure of Temporal Cavity Solitons via Intensity Modulation of the Cavity Driving Field. *arXiv* (2018), 1802.07428 (cited on page 1).
- [5] Jae K Jang, Miro Erkintalo, Stephane Coen, and Stuart G Murdoch. Temporal tweezing of light through the trapping and manipulation of temporal cavity solitons. *Nature Communications* **6** (2015), 7370 (cited on pages 1, 3, 9).
- [6] Ewelina Obrzud, Steve Lecomte, and Tobias Herr. Temporal solitons in microresonators driven by optical pulses. *Nature Photonics* **11** (2017), 600–607 (cited on pages 1, 15).
- [7] Hansuek Lee, Tong Chen, Jiang Li, Ki Youl Yang, Seokmin Jeon, Oskar Painter, and Kerry J. Vahala. Chemically etched ultrahigh-Q wedge-resonator on a silicon chip. *Nature Photonics* **6** (2012), 369–373 (cited on page 6).
- [8] Jordan R Stone, Travis C Briles, Tara E Drake, Daryl T Spencer, David R Carlson, Scott A Diddams, and Scott B Papp. Thermal and Nonlinear Dissipative-Soliton Dynamics in Kerr Microresonator Frequency Combs. *arXiv* (2017), 1708.08405 (cited on page 6).
- [9] Ian Hendry, Wei Chen, Yadong Wang, Bruno Garbin, Julien Javaloyes, Gianluca Oppo, Stéphane Coen, Stuart G Murdoch, and Miro Erkintalo. Spontaneous symmetry breaking and trapping of temporal Kerr cavity solitons by pulsed or amplitude-modulated driving fields. *Physical Review A* **97** (2018), 053834 (cited on page 12).
- [10] François Leo, Stéphane Coen, Pascal Kockaert, Simon-Pierre Gorza, Philippe Emplit, and Marc Haelterman. Temporal cavity solitons in one-dimensional Kerr media as bits in an all-optical buffer. *Nature Photonics* **4** (2010), 471–476 (cited on page 15).

- [11] Danielle Braje, Leo Hollberg, and Scott Diddams. Brillouin-Enhanced Hyperparametric Generation of an Optical Frequency Comb in a Monolithic Highly Nonlinear Fiber Cavity Pumped by a cw Laser. *Physical Review Letters* **102** (2009), 193902 (cited on page 15).
- [12] Wei Zhang, Daniel C. Cole, and Scott B. Papp. Forthcoming (2018) (cited on page 15).
- [13] Su-Peng Yu, Hojoong Jung, and Scott B. Papp. Forthcoming (2018) (cited on page 16).